Pressure-Denatured State of *Escherichia coli* Ribonuclease HI As Monitored by Fourier Transform Infrared and NMR Spectroscopy†

Kazuhiko Yamasaki,‡,§ Yoshihiro Taniguchi,|| Naohiro Takeda,||,⊥ Kayoko Nakano,|| Tomoko Yamasaki,‡,§ Shigenori Kanaya,‡,# and Motohisa Oobatake*,‡,@

Protein Engineering Research Institute, 6-2-3 Furuedai, Suita, Osaka 565-0874, Japan, and Department of Chemistry, Faculty of Science and Engineering, Ritsumeikan University, 1-1-1 Nojihigashi, Kusatsu, Shiga 525-8577, Japan

Received May 6, 1998; Revised Manuscript Received October 12, 1998

ABSTRACT: Pressure denaturation of *Escherichia coli* ribonuclease HI (RNase HI) was studied by Fourier transform infrared (FTIR) and two-dimensional NMR spectroscopy at pD* 3.0 and 25 °C. A reversible transition in the pressure range of 0.1−1090 MPa was observed with second-derivative FTIR experiments. A cooperative and gradual denaturation, involving both the secondary and tertiary structures, was observed between 240 and 450 MPa. The two peaks at 1629 and 1652 cm^{-1}, due to β-strands and α-helices, respectively, did not fully disappear after the denaturation, and are different from the spectra of the random coil peptides. The hydrogen−deuterium exchange rates of the individual backbone amide protons were determined by heteronuclear NMR combined with the pressure-jump technique at 500, 650, and 850 MPa. Although most of the amides protected in the native structure are also highly protected in the pressure-denatured state, the rate constants (0.048 ± 0.007 min^{-1}) for the amide protons at 500 MPa are similar regardless of their locations, which is an indication of the EX1 mechanism of hydrogen−deuterium exchange. The pressure-denatured state of RNase HI at 500 MPa represents a novel denatured state, which is different from a typical molten globule state at atmospheric pressure (0.1 MPa), from the viewpoint of the homogeneous rate constants. The observations at 650 MPa are essentially the same as those at 500 MPa. However, at 850 MPa, the amide exchange rates for the highly hydrophobic C-terminal half of α-helix I are significantly slower than those for the other part of the protein, which can be interpreted as a hydrophobic collapse centered at the C-terminal half of α-helix I.

The application of high pressure to a protein in an aqueous solution causes the polypeptide backbone to unfold, because the partial molar volume of a protein in the unfolded state is smaller than that in the native state (*1*, *2*). Recently, the structural and dynamical behaviors of proteins at high pressure have been investigated using several techniques, such as Fourier transform infrared (FTIR)[1] spectroscopy (*3*−*7*), NMR (*8*−*14*), and molecular dynamics simulations (*15*−*17*).

FTIR spectroscopy combined with resolution enhancement methods, like the second derivative, is one of the most powerful techniques for observing the secondary structures of proteins in aqueous solutions (*18*). This provides a sensitive diagnostic tool for monitoring the structural changes of proteins at high pressure, beyond 1000 MPa (*19*). Two-dimensional (2D) NMR spectroscopy is useful for obtaining the hydrogen−deuterium (H−D) exchange rates of individual backbone amide protons under high pressure when combined with the pressure-jump method, with which local structural changes can be elucidated (*10*, *20*−*24*). Therefore, when we study the denaturation of proteins by FTIR and 2D NMR spectroscopy under high pressure, we can obtain information about the pressure-induced unfolding of the global as well as the local structures of the protein.

Although there have been several investigations of high-pressure-induced denatured states of proteins, no consistent picture has been obtained. For example, studies with FTIR showed that pressure-denatured ribonuclease A (RNase A) and RNase S contain no residual secondary structure elements (*3*, *4*). On the other hand, an NMR study (*10*) of pressure-denatured RNase A provided information about noncooperative unfolding and partially folded structures, like

† This work was supported in part by Grants 08045025 and 09261238 from the Ministry of Education, Science and Culture of Japan (to Y.T. and M. Kato) and from the High-Tech. Research Center in Japan (to Y.T. and M. Kato).

* To whom correspondence should be addressed. Telephone: +81-52-832-1151. Fax: +81-52-832-1170. E-mail: oobatake@meijo-u.ac.jp.

‡ Protein Engineering Research Institute.

§ Present address: AIST-NIBHT CREST Centre of Structural Biology, Higashi 1-1, Tsukuba 305-0046, Japan.

|| Ritsumeikan University.

⊥ Present address: Ashigara Research Institute, Fujifilm, 210, Nakanuma, Minamiashigara, Kanagawa 250-0123, Japan.

Present address: Department of Material and Life Science, Graduate School of Engineering, Osaka University, 2-1, Yamadaoka, Suita, Osaka 565-0871, Japan.

@ Present address: Faculty of Science and Technology, Meijo University, 1-501, Shiogamaguchi, Tenpaku-ku, Nagoya 468-8502, Japan.

[1] Abbreviations: FTIR, Fourier transform infrared; GdnDCl, guanidine deuteriochloride; H−D exchange, hydrogen−deuterium exchange; HSQC, heteronuclear single-quantum coherence; NMR, nuclear magnetic resonance; pD*, pD value read with a pH meter without correction; RNase HI, ribonuclease HI (EC 3.1.26.4); 2D, two-dimensional.

10.1021/bi981046w CCC: $15.00
Published on Web 12/01/1998

the molten globule state. Likewise, in the case of bovine pancreatic trypsin inhibitor (BPTI), the secondary structures of the pressure-denatured state derived from different experiments are inconsistent with each other. When the pressure was increased up to 1000 MPa, the fluorescence intensity of tyrosine observed by Scarlata (cited in Figure 9 of ref *15*) and FTIR experiments (*7*) did not reveal any pressure-induced unfolding of the protein. In contrast, an FTIR experiment (*5*) at 1500 MPa showed a pressure-induced, gradual transformation from an α-helical and unordered structure to the β-sheet structure. Therefore, it is essential to obtain a consistent view of the pressure-denatured structures of proteins.

Escherichia coli RNase HI, which specifically hydrolyzes the RNA strand of RNA−DNA hybrids, is a small globular protein with 155 amino acid residues. We have used this protein for studies of protein stability (*25*−*37*) and folding mechanisms (*38*−*40*). It consists of five α-helices and five β-strands, and has an α-helical content of 40% and a β-sheet content of 28%, as determined by X-ray crystallography (*41*, *42*). RNase HI is suited to these studies for the following reasons. (i) Highly refined coordinates of this protein are available, as determined by X-ray crystallography (*41*−*43*). (ii) The assignments of the NMR signals and the pK_a values of the amino acid residues, as well as the determination of the secondary structure in an aqueous solution, have been completed (*44*−*47*). (iii) An overproduction system for this protein is available (*26*). (iv) It reversibly unfolds in a single cooperative fashion with thermal and chemical denaturations (*28*, *48*). (v) H−D exchange analyses on the native state and the folding intermediate of the wild-type protein (*40*, *49*), as well as those on a cysteine-free mutant protein in the native, acid-denatured, and folding intermediate states, have been reported (*50*−*52*).

In this article, we monitored the pressure-induced reversible denaturation of *E. coli* RNase HI using high-pressure FTIR spectroscopy and investigated the secondary structure of the polypeptide backbone at high pressure. To obtain specific structural information on the pressure-denatured RNase HI, we also used the H−D exchange kinetics observed by 2D ^{1}H−^{15}N NMR spectroscopy to determine the protection factors of the individual backbone amide protons of RNase HI. Interpretations of the observations by the two methods are discussed.

MATERIALS AND METHODS

Sample Preparation. E. coli RNase HI uniformly labeled with ^{15}N was prepared as described previously (*53*). D_2O (99.8 at. % D) and DCl (99 at. % D) were purchased from CEA-ORIS Bureau des Isotopes Stables and Sigma Chemical Co., respectively. All other materials were of reagent grade.

Deuterated RNase HI for FTIR Measurements. When a high concentration of RNase HI is dialyzed against distilled water (pH 7), precipitation is frequently observed. The protein solution is stable at pH 5.5 (*26*) and does not precipitate. The purified protein solution (2.2 mg/mL) in 10 mL of 50 mM sodium acetate buffer (pH 5.5) was concentrated until the volume of the protein was reduced to 400 μL, using a Centricon 10 unit (Amicon). Two milliliters of D_2O buffer [10 mM CD_3COONa (CIL), the pD value read by pH meter without correction (pD*) was 5.5] was added to the resultant protein solution. To prepare the deuterated and denatured protein solution, deuterated GdnDCl was dissolved in the solution to a final concentration of 4 M, at which the protein is denatured. The solution was left at 4 °C overnight to allow the deuteration of the protein to be complete. The solution was then diluted by 4-fold, to reduce the GdnDCl concentration, by adding 50 mM CD_3COONa/D_2O buffer (pD* 5.5) for refolding. The solution was subjected to ultrafiltration against the same buffer, using a Centricon 10 unit to eliminate the GdnDCl. Finally, the buffer of the protein solution was replaced with D_2O/DCl (pD* 3.0) to remove the CD_3COO^-, which influences the FTIR spectra, using a Centricon 10 unit, and the protein solution was lyophilized. The completion of the deuteration was confirmed by the frequency shift of the amide II band from 1550 to 1450 cm^{-1}, as a result of the deuteration of the backbone amide groups (*19*). The sample solution was prepared by dissolving the lyophilized RNase HI in 10 μL of D_2O/DCl (pD* 3.0) for the pressure experiments. All sample solutions were prepared just before the FTIR measurements. It took approximately 1 h to record the first infrared spectrum after the sample preparation.

High-Pressure FTIR Measurements. For the high-pressure experiments, the sample solutions were placed together with a small amount of powdered α-quartz in a 1.0 mm diameter hole of a 0.05 mm thick stainless steel (SUS 304) gasket mounted on a diamond anvil cell (*54*). The α-quartz was used as an internal pressure calibrant (*54*). Infrared spectra of the samples at pressures of up to 1090 MPa, by means of the diamond anvil cell, were recorded at 25 °C using a Perkin-Elmer 1725X FTIR spectrometer equipped with a liquid nitrogen-cooled MCT (HgCdTel) detector. The infrared beam was condensed by a zinc selenide lens system onto the sample in the diamond anvil cell. For each spectrum, 1000 interferograms were co-added and analyzed by Fourier transformation to give a spectral resolution of 2 cm^{-1}. The samples were allowed to equilibrate at the chosen pressure for 30 min prior to each infrared measurement, which took 16 min. The pressure was increased or decreased at an average rate of approximately 150 MPa/h. The temperature was controlled to within 0.2 °C by a circulating water jacket. To eliminate the spectral contributions of atmospheric water vapor, the spectrometer and the sample chamber were continuously purged with dry air.

Resolution Enhancement Technique. Each difference spectrum of RNase HI in solution was obtained by digitally subtracting the appropriate reference spectrum of the medium from the spectrum of each sample solution. The bands originating from water vapor in the second-derivative infrared spectrum were subtracted until the absorption-free region of the amide I (I′) band above 1700 cm^{-1} was featureless. Second-derivative spectra were generated by using a nine-data point (9 cm^{-1}) Savitzky−Golay function, available in the Perkin-Elmer software, IRDM2.

Pressure-Jump Method. The measurement of the amide H−D exchange rate under pressure was carried out by a modification of the method described by Baum et al. (*55*). Four milligrams of the protein samples was dissolved in 400 μL of pH-adjusted water (pH 3.0) by ultrafiltration using a Centricon 10 unit and lyophilized. They were dissolved again in 3.5 mL of D_2O buffer [10 mM CD_3COONa (pD* 3.0)] and were packed quickly in a Teflon container. The sample

container was placed in a high-pressure vessel (Hikari Koatsu Co. Ltd. HR15-B2 type, maximum pressure of 1500 MPa) maintained at 25 ± 0.2 °C. The sample was pressurized to 500 MPa from 0.1 MPa for about 10 min, during which the protein denaturation was expected to be essentially completed. After incubations for 0, 15, 30, 60, 120, and 240 min, the samples were depressurized to 0.1 MPa from 500 MPa for about 5 min. The refolded protein solutions were cooled on ice and lyophilized. Within 5 h of the NMR measurement, the samples were dissolved in 200 μL of a D_2O solution [100 mM CD_3COONa (pD* 5.5)] with a Centricon 10 unit. This procedure was carried out at 4 °C to minimize the extent of amide H−D exchange during the process. The experiments at 650 and 850 MPa were performed similarly.

NMR Measurements and Data Processing. NMR spectra were measured on a Bruker AM-500 spectrometer. Proton and nitrogen chemical shifts were determined relative to sodium 2,2-dimethyl-2-silapentane-5-sulfonate and liquid NH_3, respectively. To correlate the ^1H and ^{15}N shifts, two-dimensional heteronuclear single-quantum coherence spectroscopy (HSQC) (*56*) was carried out with a coupling delay of 2.25 ms. The sweep width for ^1H was 7042 Hz, and that for ^{15}N was 1830 Hz. GARP1 ^{15}N decoupling (*57*) was employed during the detection period. Free induction decays (48 scans) of 2K data points in the t_2 domain were collected for 200 data points in the t_1 domain using time-proportional phase incrementation (*58*). Data processing was achieved using the FELIX 2.30 software (Biosym) on an IRIS indigo II computer (Silicon Graphics). With squared-sine bell windows of 60° for the t_2 and 90° for the t_1 dimension, followed by zero-filling and Fourier transformation, spectra of 2048 × 512 data points were obtained. The cross-peak intensities of the refolded proteins after the pressure-jump processes were measured. To normalize the intensities, those of the δ-methyl proton of Ile 116 in one-dimensional NMR were measured and used as the standard before observing each 2D HSQC spectrum.

Analysis of H−D Exchange Data. The cross-peak intensities normalized against six time points were fitted to a single-exponential function

$$I(t) = I_0 \exp(-kt) + I_\infty \quad (1)$$

where $I(t)$ is the normalized cross-peak intensity as a function of the incubation time t, I_0 and I_∞ are the initial and the steady-state values of the intensities, respectively, and k is the exchange rate constant. Fitting was carried out with a FORTRAN77 program employing the nonlinear least-squares minimization algorithm of the Levenberg−Marquardt method (*59*, *60*) in an IMSL library (IMSL Inc.) on a VAX computer (DEC). To estimate the uncertainty of the relaxation times, a Monte Carlo simulation (*61*, *62*) was carried out as follows. While the peak intensities of the time points were randomized as Gaussian distributions, using an algorithm in the IMSL library, eq 1 was refitted 500 times. For the standard deviations of the peak intensities, either the larger value of the root-mean-square baseline noise of the HSQC spectra or the residuals of the first fitting were employed. The average and the standard deviation of the ensemble of the rate constants were adopted for its absolute value and uncertainty, respectively.

The intrinsic exchange rates (k_{int}) of amide protons at 500, 650, and 850 MPa, pD* 3.0, and 25 °C were obtained by methods of Bai et al. (*63*) and Zhang et al. (*10*). The intrinsic exchange rate is the sum of the contributions from the exchange reactions catalyzed by acid (k_a), base (k_b), and water (k_w) and can be expressed by

$$k_{int} = k_a[D^+] + k_b[OD^-] + k_w \quad (2)$$

If a constant activation volume and a constant activation energy are assumed for the intrinsic amide exchange, each exchange rate at a particular temperature and pressure is corrected by

$$k_i(T,P) = k_i(T_0,P_0) \exp[-E_i(1/T - 1/T_0)/R] \times \exp[-\Delta V^{\#}_i(P - P_0)/RT] \quad (3)$$

where i is a (acid), b (base), or w (water) and R is the gas constant. The values for the activation energies are as follows: E_a = 14 kcal/mol, E_b = 17 kcal/mol, and E_w = 19 kcal/mol (*63*). The activation volumes ($\Delta V^{\#}$) for the acid- and base-catalyzed reactions are known to be 0 ± 1 and 6 ± 1 mL/mol (*64*) in random coil poly-D,L-lysine at pH 3.5. The activation volume for water autoionization is −21.2 mL/mol (*65*), which was used instead of −20.4 mL/mol (*10*, *64*).

Using the method of Bai et al. (*63*), one can distinguish the charges of Asp, Glu, and His residues, the disulfide-bonded Cys residues, and the cis−trans isomerization of Pro residues. It was assumed for the pressure-denatured state of RNase HI at pD* 3.0 that all of the Asp and Glu residues are not ionized, the His residues are charged, and all Pro residues are in the trans conformation. It has been shown that RNase HI lacks disulfide bonds (*41*, *66*).

RESULTS AND DISCUSSION

Assignments of the Amide I′ Component Bands for Deuterated RNase HI. The infrared spectra in the amide I′ region of the amide-deuterated RNase HI in D_2O solution (pD* 3.0) at 25 °C are shown in Figure 1a. The amide I′ region corresponds to the amide I region for the peptide in H_2O, and this region is sensitive to the secondary structure. The original infrared spectrum shows a broad and asymmetric band with the maximum peak at approximately 1650 cm^{-1} (Figure 1a). This is the result of the overlapping of a number of individual amide I′ component bands at the frequencies characteristic of different secondary structure elements. The second-derivative analysis clearly indicated that the amide I′ bands are separated directly into the component bands (Figure 1b). Absorbance bands in the original spectrum are revealed as negative bands in the second-derivative spectrum. On the basis of the reported FTIR spectroscopic studies of globular proteins (*18*, *67*−*71*), the component bands of the amide I′ bands for the deuterated RNase HI (Figure 1b) are assigned to the secondary structures, as described below. The negative peaks at 1629 and 1687 cm^{-1} are assigned to β-structures. The negative peak at 1652 cm^{-1} is assigned to α-helices. Those at 1670 and 1677 cm^{-1} are assigned to turns. The peak at 1607 cm^{-1} is mainly assigned to the side chains of tyrosine residues (*72*, *73*). Recent studies (*74*−*76*) have indicated that the bands observed in the 1638−1640 cm^{-1} region arise from 3_{10}-helices, rather than from extended strands as previously proposed (*67*). The X-ray

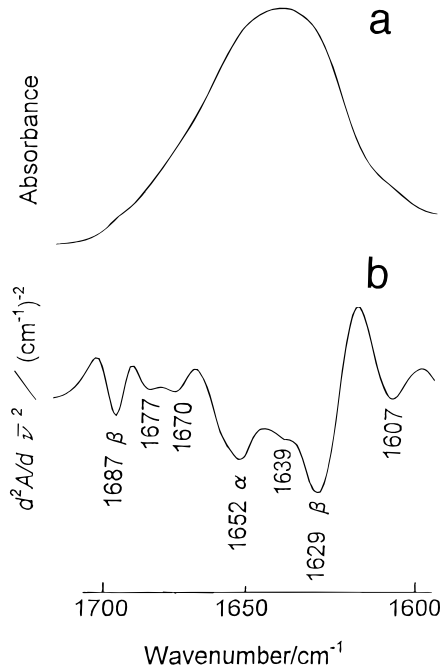

FIGURE 1: Original (a) and second-derivative (b) infrared spectra in the amide I′ region of deuterated RNase HI at 25 °C and 0.1 MPa. The RNase HI was dissolved in D_2O/DCl at pD* 3.0, and the protein concentration was 50 mg/mL.

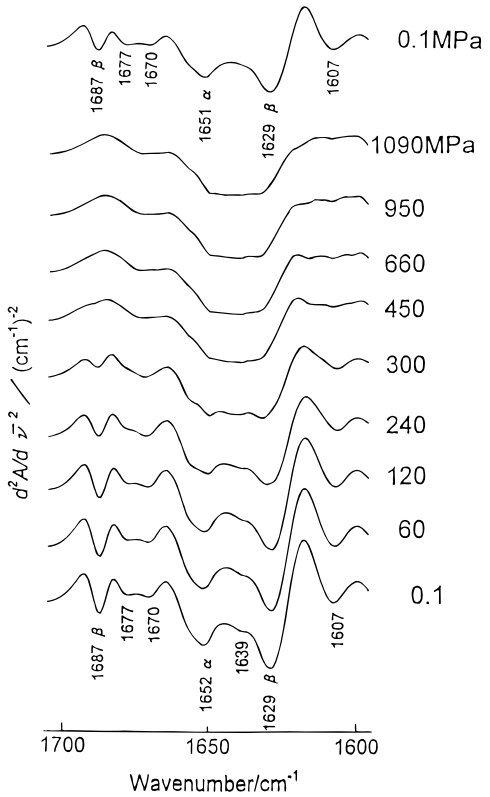

FIGURE 2: Second-derivative infrared spectra in the amide I′ region of deuterated RNase HI upon a pressure increase at 25 °C and pD* 3.0. Solution conditions are the same as those described in the legend of Figure 1. The pressure was increased from 0.1 (bottom) to 1090 MPa and was decreased to 0.1 MPa (top).

structure (*42*) indicates that RNase HI contains three 3_{10}-helices, with a content of 10%. From these results, the small peak at 1639 cm^{-1} may be assigned to the 3_{10}-helices. The relative intensities of the amide I′ component bands at 1629 and 1652 cm^{-1} are stronger than those of the other component bands of the tyrosine side chains and the turns, which suggests that α-helix and *β*-sheet secondary structures predominate over the turns in RNase HI. In fact, the reverse turn content (13%) obtained from the X-ray structure (*42*) is lower than that of α-helix and *β*-sheet.

Pressure-Induced Changes in the FTIR Spectra of RNase HI. Figure 2 shows the second-derivative infrared spectra of deuterated RNase HI at various pressures, from 0.1 to 1090 MPa, at pD* 3.0 and 25 °C. The changes in the amide I′ bands shown in Figure 2 are a direct indication of the pressure-induced changes in the secondary structure of RNase HI, because no further amide deuteration occurs. At pressures of up to 1090 MPa, there are small frequency shifts in all of the amide I′ component bands, within the experimental error of 2 cm^{-1}, and no significant changes in the amide I′ band contour are observed. A further increase in pressure, from 240 to 450 MPa, induces the cooperative and gradual decrease of the intensities of all of the amide I′ component bands of native RNase HI (Figure 2). This clearly indicates that the pressure induces cooperative denaturation of the secondary structure elements. It should be noted, however, that the two peaks at 1629 and 1652 cm^{-1}, due to the *β*-strands and the α-helices, respectively, appear to remain as shoulders of a broad band even when the pressure was increased beyond 450 MPa, and did not disappear at the highest pressure of 1090 MPa. This indicates that the pressure-denatured state may contain residual secondary structure.

A random coiled polypeptide of poly-L-glutamic acid in aqueous solution at atmospheric pressure (0.1 MPa) (*77*) and high pressure (1080 MPa) (*3*) and the completely pressure-unfolded RNase A (*3*) show second-derivative IR spectra with broad bands centered at approximately 1640 cm^{-1} without any shoulders, as shown in Figure 3. The spectra of RNase HI at pressures above 450 MPa are clearly different from these random coil spectra, which supports the possibility of residual secondary structure. It should be noted that this putative residual structure consists of both α-helix and *β*-sheet.

The band of Tyr side chains at 1607 cm^{-1} almost disappeared at pressures higher than 450 MPa, and the disappearance of this band correlates with the pressure-induced change in the secondary structure of RNase HI. RNase HI contains five Tyr residues, as shown in Figure 4. These Tyr residues are almost completely buried inside the protein molecule and play an important role in the packing among the secondary structures. The disappearance of the band mainly assigned to the Tyr side chains indicates that the highly specific interactions among the secondary structures in the native structure are largely disrupted at pressures higher than 450 MPa. Since the pressure-denatured RNase HI is likely to have some residual secondary structural elements at pressures above 450 MPa, we may say that the pressure-denatured RNase HI exhibits the characteristics of a molten globule, which is a compact, denatured structure with a significant amount of secondary structure but a largely disordered tertiary structure (*78*, *79*).

At high pressure, gelation was observed for RNase A at 1240 MPa (*3*) and for RNase S at 1160 MPa (*4*). In contrast, aggregation or gelation of a protein solution of RNase HI was not observed at the highest pressure, 1090 MPa. The pressure-induced changes in the secondary structure of RNase

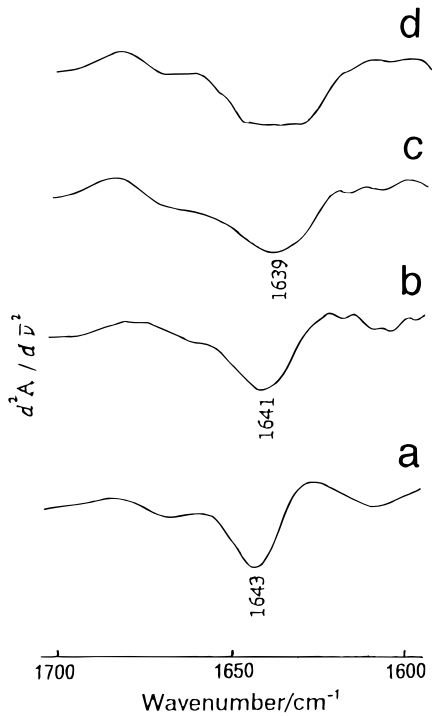

FIGURE 3: Second-derivative infrared spectra in the amide I′ region of poly-L-glutamic acid at 30 °C and 0.1 MPa (a) and 30 °C and 1080 MPa (b), of completely pressure-unfolded RNase A at 30 °C and 1030 MPa (c), and of deuterated RNase HI at 25 °C and 1090 MPa (d). Spectra a−c are adapted from Takeda et al. (*3*). Poly-L-glutamic acid sodium salt and RNase A were dissolved in 0.05 M Tris-DCl/D_2O buffer at pD* 7.0, and both concentrations were 50 mg/mL.

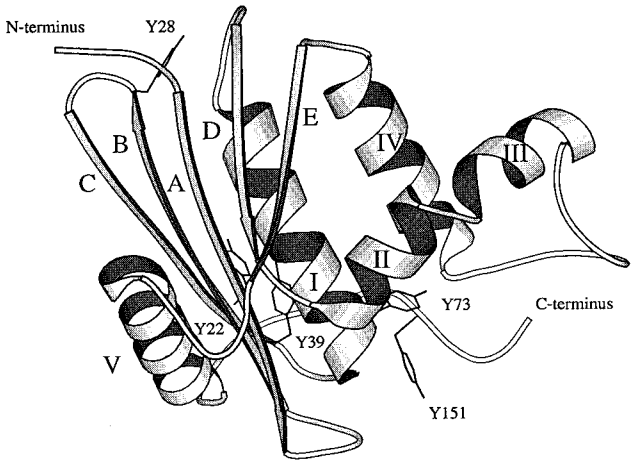

FIGURE 4: Ribbon representation of the polypeptide backbone of RNase HI drawn with the program MOLSCRIPT (*95*). The polypeptide backbone is composed of a five-stranded β-sheet (A−E) and five α-helices (I−V). The major domain comprises four α-helices (I, II, IV, and V) and one large β-sheet consisting of three antiparallel β-strands (A−C) at the amino terminus as well as three parallel β-strands (A, D, and E). Tyr 22, Tyr 28, and Tyr 39 are located in antiparallel strands βB, βB, and βC, respectively. Tyr 73 is located in α-helix II joined with α-helix III. Tyr 151 lies in a coil region just near the C-terminus. The accessible surface areas (ASA) of the Tyr residues of RNase HI (*42*), calculated by our method (*96*, *97*), are 10.2, 15.8, 16.5, 23.5, and 33.1 Å^2 for Tyr 22, 28, 39, 73, and 151, respectively, and their ratios of ASA in the native state to those in the extended state are 4.6, 8.1, 8.5, 12.5, and 15.9%, respectively, indicating that these Tyr residues are almost fully buried inside the protein molecule.

HI were completely reversible at pD* 3.0, as the amide I′ band contour, after the pressure was reduced to 0.1 MPa, is

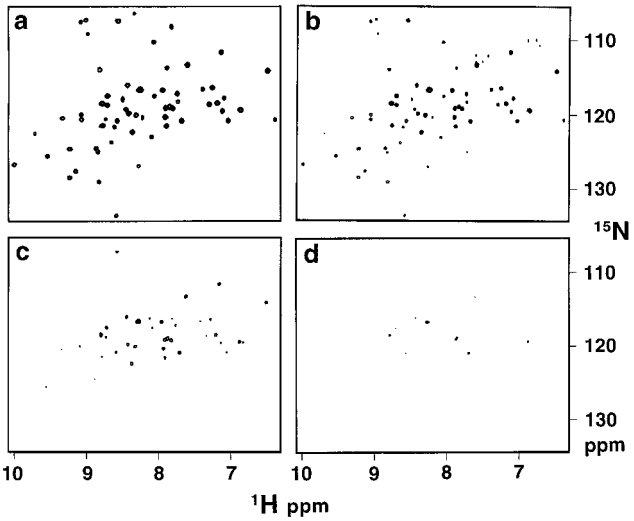

FIGURE 5: ^{1}H−^{15}N HSQC spectra of RNase HI after the pressure-jump process. Samples were incubated at 500 MPa, 25 °C, and pD* 3.0 for (a) 0, (b) 15, (c) 30, and (d) 60 min. The plotting levels were normalized according to the protein concentration. The RNase HI was dissolved in D_2O/CD_3COONa at pD* 3.0, and the protein concentration was 20 mg/mL.

identical with that observed before the pressure was applied. The thermal denaturation at pH 3.0 in a dilute solution (0.1 mg/mL), observed by circular dichroism, also shows full reversibility (*48*), which may be due to electrostatic repulsion between two monomers, because the RNase HI protein has an isoelectric point of 9.0 (*80*).

NMR H−D Exchange Rates at a High Pressure of 500 MPa. To determine the H−D exchange rates of the protein at an atomic resolution, a pressure-jump experiment with NMR was performed at 500 MPa. Figure 5 shows the 2D ^{1}H−^{15}N HSQC spectra of the native RNase HI samples after the incubation at 500 MPa. The chemical shifts of the observed cross-peaks are almost the same as those of the intact protein, which shows that the denaturation by the pressure is fully reversible, in agreement with the FTIR data (Figure 2). The assignments of the cross-peaks by Yamazaki et al. (*44*) were easily applied to these spectra. Among the 149 backbone amide protons in RNase HI (the N-terminus and the five Pro residues were excluded from the 155 residues), 61 amide protons were significantly protected from the H−D exchange in the native structure (the protection factors were 10^3−10^8) at pH 5.5 and 27 °C in the native state (*49*). Among these 61 protons, 58 peaks at 500 MPa were observed separately in the D_2O solution, as shown in Figure 5. Those of Val 5, Gly 38, and Thr 69 were not observed, probably because of their relatively weak protection in the native state, of which protection factors are less than 2600 (*49*). The analyzed residues cover most of the secondary structural elements, such as α-helices I−V and β-strands A−E, as well as residues in loops, such as Gly 18, Thr 42, and Leu 146, which form hydrogen bonds in the native structure (*42*).

The H−D exchange during the incubation at 500 MPa decreases the cross-peak intensities of the protein samples (Figure 5a−d) depending on the incubation time. The dependence of the intensities on the incubation time fits very well to single-exponential curves, as shown in Figure 6. The observed rate constants (k_{obs}) of each residue in the pressure-denatured state at 500 MPa and 25 °C are shown in Figure

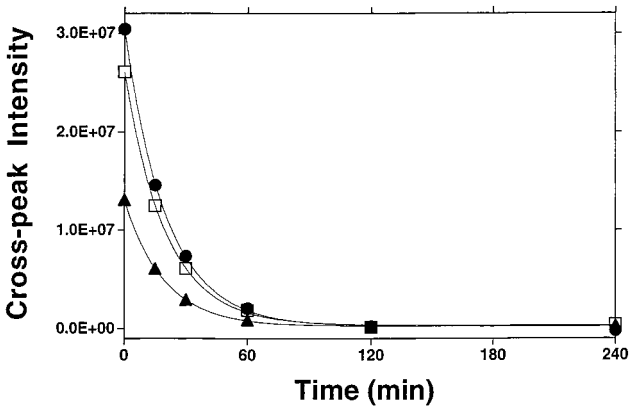

FIGURE 6: Cross-peak intensities of Gly 21 (▲), Ala 52 (●), and Leu 136 (□), as functions of the incubation times at 500 MPa, with the single-exponential best-fit curves.

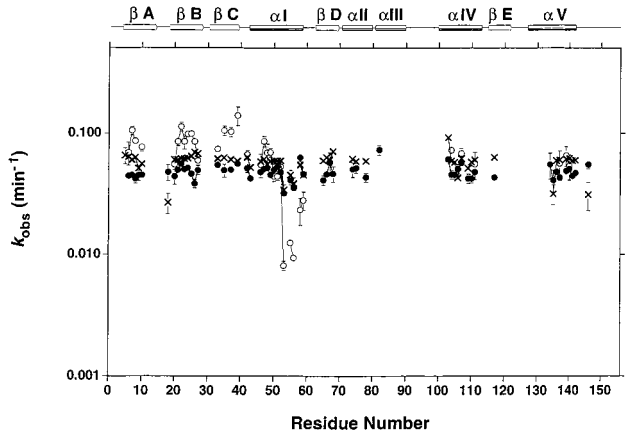

FIGURE 7: Rate constants and error bars for the H−D exchange in the pressure-denatured state as a function of residue number at 500 (●), 650 (×), and 850 MPa (○) (25 °C and pD* 3.0).

7 and Table 1. The rate constants range from 0.032 ± 0.002 (Ile 53) to 0.073 ± 0.007 min^{-1} (Ile 82). The average and the standard deviation for all of the analyzed residues are 0.048 and 0.007 min^{-1}, respectively. Surprisingly, the rate constants for the amide protons show similar values, regardless of their locations in the tertiary structure. All the k_{obs} values are significantly smaller than the exchange rates for unstructured peptides (intrinsic exchange rates, k_{int}), calculated according to the methods of Bai et al. (*63*) and Zhang et al. (*10*) (Table 1). This indicates that amide protons of all the observed residues are significantly protected from the solvent exchange.

The scheme of the H−D exchange reactions for protected protons can be depicted as follows (*21*):

$$\mathrm{P} \underset{k_{cl}}{\overset{k_{op}}{\rightleftharpoons}} \mathrm{O} \xrightarrow{k_{int}} \text{exchange} \qquad (4)$$

where P is the major protected conformation, O is the unprotected open conformation, with a minor population, k_{op} and k_{cl} are the rate constants for the opening and closing events, respectively, of the protected amides, and k_{int} is the intrinsic exchange rate constant. We assume that the major protected conformation is the pressure-denatured state and that the contribution of the residual native state is negligible after preincubation for about 10 min, which is consistent with the single-exponential curves for the decrease in peak intensities (Figure 6). There are two simplified mechanisms for the H−D exchange reaction corresponding to two extreme conditions, EX1 ($k_{int} \gg k_{cl}$) and EX2 ($k_{cl} \gg k_{int}$) (*21*). The observed exchange rate equals k_{op} in the EX1 mechanism, while it is k_{int} (k_{op}/k_{cl}) in the EX2 mechanism.

Table 1: Observed (k_{obs}) and Intrinsic (k_{int}) Exchange Rates of Amide Protons of RNase HI at 500 MPa and k_{obs} at 650 and 850 MPa (25 °C and pD* 3.0)

		500 MPa		650 MPa	850 MPa
residue	sec. str.[a]	k_{obs} x 10^2 (min^{-1})	k_{int} x 10^2 (min^{-1})	k_{obs} x 10^2 (min^{-1})	k_{obs} x 10^2 (min^{-1})
E6	βA	4.4	527	6.4	6.9
I7	βA	4.5	191	6.0	10.5
F8	βA	4.2	142	6.3	8.6
T9	βA	4.5	409	5.1	ND[c]
D10	βA	4.5	3250	5.6	7.7
G18	loop	4.8	449	2.7	ND
G20	βB	4.4	449	6.0	5.5
G21	βB	5.0	1150	6.0	8.5
Y22	βB	5.6	334	6.2	11.3
G23	βB	5.0	874	6.2	8.5
A24	βB	5.2	623	6.2	9.8
I25	βB	4.6	78	6.5	9.9
L26	βB	3.8	65	6.9	8.5
R27	βB	5.0	311	6.8	5.9
K33	βC	5.5	937	6.2	7.4
F35	βC	5.0	382	6.3	10.5
A37	βC	5.0	836	6.1	10.3
Y39	βC	5.6	334	5.9	14.0
T42	loop	5.2	591	6.4	6.7
T43	αI	4.3	564	5.3	ND
R46	αI	4.8	1050	5.8	5.5
M47	αI	5.1	679	6.1	8.6
E48	αI	5.2	937	5.6	6.9
L49	αI	4.6	270	5.9	7.0
M50	αI	5.0	252	5.9	4.4
A51	αI	5.3	540	5.9	4.4
A52	αI	4.8	421	6.0	5.3
I53	αI	3.2	78	3.4	0.8
A55	αI	4.1	304	4.5	1.3
L56	αI	3.6	111	3.9	0.9
A58	αI	6.3	1030	5.5	2.3
L59	loop[b]	4.6	111	4.5	2.8
V65	βD	4.1	205	6.0	ND
I66	βD	4.6	57	6.3	ND
L67	βD	5.7	65	6.1	5.8
S68	βD	4.6	605	7.1	ND
V74	αII	5.1	94	6.1	ND
R75	αII	5.2	365	5.9	ND
I78	αII	4.3	116	5.9	ND
I82	αIII	7.3	61	ND	ND
L103	αIV	6.1	438	9.2	ND
W104	αIV	4.6	101	5.9	7.3
Q105	αIV	4.5	373	5.8	ND
R106	αIV	5.1	797	4.3	ND
L107	αIV	5.7	183	6.2	6.8
A109	αIV	4.2	1670	5.2	ND
A110	αIV	4.2	421	5.8	ND
L111	αIV	4.8	111	6.0	5.6
K117	βE	4.3	225	6.3	ND
D134	αV	5.5	727	ND	ND
E135	αV	4.1	289	3.2	ND
L136	αV	4.8	270	6.0	ND
A137	αV	4.3	260	6.0	5.6
A139	αV	4.9	695	6.1	6.5
A140	αV	5.1	421	6.2	5.4
A141	αV	4.4	421	5.9	ND
M142	3_{10}III	4.7	409	6.0	ND
L146	loop	5.5	175	3.1	ND

[a] Secondary structure defined in the crystal structure (*42*); αI−V, α-helices I−V; βA−E, β-strands A−E; 3_{10}III, 3_{10}-helix III. [b] C-Terminal cap of α-helix I. [c] ND means not determined.

In the EX1 mechanism, k_{obs} does not depend on k_{int}, while it depends on k_{int} in EX2. In the pressure-denatured state of RNase HI, the k_{obs}'s have similar values, regardless of the variation in k_{int} as shown in Figure 7 and Table 1, which indicates that the k_{obs} values do not depend on k_{int}. Thus, it is appropriate to assume the EX1 mechanism, rather than the EX2 mechanism, for the H−D exchange in the pressure-denatured state. The EX1 condition ($k_{int} \gg k_{cl}$) is partly brought about by the acceleration of k_{int} by the increase in pressure.

Since the rates of the opening events, k_{op}, are similar for all residues, the transition from the P state to the O state should open all the protected amide protons with equal probabilities. This may be a global reaction which involves all the residues, or a set of local reactions which occur at all the residues with equal probabilities. In contrast, the H−D exchange under the native conditions is more complicated, and involves the local opening events and the transition between the native and the intermediate states, as well as the global unfolding, for which the EX2 mechanism was assumed (*49*, *50*). It should be noted that the protection factor (k_{int}/k_{obs}) represents the intensity of the protection when the EX2 mechanism is assumed ($k_{int}/k_{obs} = k_{cl}/k_{op}$), while it is physically meaningless under the EX1 condition at 500 MPa.

Structure of Pressure-Denatured RNase HI at 500 MPa. The FTIR experiment described here indicated that the secondary structure of the pressure-denatured state of the RNase HI protein is denatured but not fully disordered, while the tertiary structure is almost fully disordered. The NMR analysis indicated that the amide groups are significantly protected from solvent exchange and that the reaction opens all the protected amide protons with equal probabilities.

To interpret these observations, a randomly packed structure with largely disordered secondary structure may be considered. The amide protection in this structure is explained by the location of the amides, which are mostly in the interior of the protein molecule. The amide exchange occurs when the interior is exposed to the solvent. Due to the randomness of the packing, the population of the exposed conformation is similar for all of the residues, which explains the similarity in the opening rates. A global transition from the packed structure to a fully unfolded, unpacked structure may also account for the conformational opening. It should be noted that the FTIR analysis suggests a residual secondary structure, consisting of α-helix and β-sheet. Presumably, some minor conformations have a small amount of the native-like secondary structure. These minor conformations essentially do not contribute to the H−D exchange rate of the major conformation.

It was theoretically proposed that compact denatured states exhibit a H−D exchange rate slower than that of fully disordered state (*81*). These states have hydrophobic clusters in the nonpolar core and have disorder in both the side chains and the backbone. On the other hand, the side chain molten globule model (*82*, *83*) has only side chain disorder. Hydrophobic clusters in denatured states have been observed in the equilibrium expanded states of lysozyme (*84*), tryptophan synthase (*85*), bovine α-lactalbumin (*86*), human α-lactalbumin (*87*), 434-repressor (*88*), and bovine pancreatic trypsin inhibitor (*89*). The pressure-denatured state at 500 MPa may correspond to the compact denatured state, with disorder of the side chains and the backbone.

Relationship with Other Nonnative Structures. The structures of the nonnative states of the RNase HI protein and its mutant, such as the folding intermediate (*40*, *52*) and the acid-denatured molten globule (*38*, *51*; K. Yamasaki et al., unpublished results), were investigated. They were classified into a typical molten globule state with highly ordered secondary structure and disordered tertiary structure.

Among the secondary structure elements, α-helix I is most highly protected and the surrounding parts, such as α-helix IV, are also well protected in the molten globules of RNase HI (*40*, *51*, *52*; K. Yamasaki et al., unpublished results). Also in other known molten globules, such as those of cytochrome *c* (*90*), guinea pig α-lactalbumin (*91*, *92*), human α-lactalbumin (*93*), and apomyoglobin (*94*), the rate constants vary for the residues that are located at different secondary structures and are explained by the EX2 mechanism. The pressure-denatured state in this study shows a completely different protection pattern, in which most of the amide groups are protected with similar exchange rates and are explained by the EX1 mechanism. Thus, a novel structural category seems to be appropriate for the pressure-denatured state of RNase HI at 500 MPa, which is different from a typical molten globule state at atmospheric pressure (0.1 MPa), from the viewpoint of the homogeneous rate constants.

Comparison with the Pressure-Denatured State of RNase A. It has been reported that the pressure-denatured RNase A adopts a compact structure and may contain partially folded secondary structures (*10*). Especially, the central region of the β-sheet, comprising residues 70−87 involved in the hydrophobic core, is relatively well protected from the solvent exchange. No significant protection was found for the residues in the α-helices, except for those located around Cys 58, which forms a disulfide bond with Cys 110. These observations are in contrast to those for RNase HI from the viewpoint of the homogeneous rate constants.

NMR H−D Exchange Rates at a High Pressure of 650 MPa. When we increase the pressure from 500 to 650 MPa, the intrinsic hydrogen exchange rate increases according to eq 3. For example, it increases from 4.21 to 15.3 min^{-1} for Ala 52, when the pressure increases from 500 to 650 MPa. The observed exchange rates at 650 MPa (Table 1 and Figure 7) are significantly slower than the corresponding intrinsic exchange rates. The average increment in the observed exchange rates from 500 to 650 MPa is approximately 20%, while the intrinsic exchange rates became 3.5 times as large. This is consistent with the assumption of the EX1 mechanism for the H−D exchange. The values at 650 MPa are also very similar, regardless of the location (Figure 7). Thus, the characteristics of the structure at 650 MPa are essentially the same as those at 500 MPa.

NMR H−D Exchange Rates at a High Pressure of 850 MPa. When we increase the pressure from 650 to 850 MPa, the intrinsic hydrogen exchange rate for Ala 52 increases from 15.3 to 86.7 min^{-1}. The observed hydrogen exchange rates at 850 MPa are also shown in Figure 7. Among the 58 amide protons analyzed at 500 MPa, 36 amide protons were also highly protected and could be analyzed at 850 MPa. In contrast to the exchange rates at 500 and 650 MPa, which are quite uniform regardless of the location, the exchange rates significantly varied at 850 MPa (Figure 7). According to the dependence of the exchange rates on the increase in the pressure, the residues are classified into three groups.

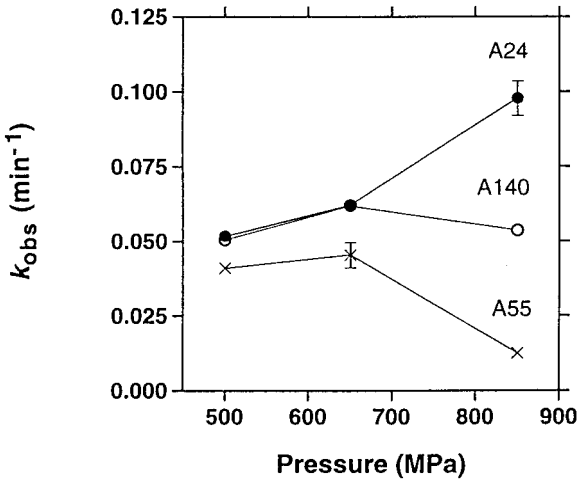

FIGURE 8: Rate constants and error bars for the H−D exchange in the pressure-denatured state as a function of pressure for Ala 24 (●), Ala 55 (×), and Ala 140 (○) (25 °C and pD* 3.0).

Typical examples representing the three groups are shown in Figure 8. The first group is the N-terminal region, which contains the secondary structures of β-strands A−C, and is represented by Ala 24. The exchange rates of the residues in this region increase when the pressure is increased from 650 to 850 MPa. The second group is the C-terminal region, which contains the secondary structures of the N-terminal part of α-helix I, β-strand D, and α-helices II, IV, and V, and is represented by Ala 140. The observed exchange rates of the residues in this region are not severely affected when the pressure is increased. The third group is the C-terminal hydrophobic part of α-helix I, Ile 53, Ala 55, Leu 56, Ala 58, and Leu 59. Surprisingly, the observed exchange rates for the residues in this region decrease when the pressure is increased. This region is the most protected among the three regions at 850 MPa.

The heterogeneous pattern of the H−D exchange protection for the amino acid residues at 850 MPa is clearly different from the patterns at 500 and 650 MPa, which is an indication of the difference in the secondary structure. The EX1 assumption does not seem to be applicable at 850 MPa. There is probably a hydrophobic collapse centered at the C-terminal half of α-helix I, with its hydrophobic residues. This would reduce the population of conformations where the residues in the C-terminal half of α-helix I are exposed to the solvent.

Since the protection pattern at 850 MPa is coincident with the results that the hydrophobic α-helix I is probably a nucleus of initial folding (*40*, *52*), the structure at 850 MPa may be related to the early stage of the folding pathway. If the heterogeneous pattern of the exchange rates is considered, the pressure-denatured structure of RNase A (*10*) is related to that of RNase HI at 850 MPa, rather than to those at 500 and 650 MPa. The structures at 500 and 650 MPa may be considered intermediates in the process of pressure denaturation.

ACKNOWLEDGMENT

We thank Dr. M. Gromiha for critical reading of the manuscript.

REFERENCES

1. Taniguchi, Y., and Suzuki, K. (1983) *J. Phys. Chem. 87*, 5185−5193.
2. Vidugiris, G. J. A., Markley, J. L., and Royer, C. A. (1995) *Biochemistry 34*, 4909−4912.
3. Takeda, N., Kato, M., and Taniguchi, Y. (1995) *Biochemistry 34*, 5980−5987.
4. Takeda, N., Kato, M., and Taniguchi, Y. (1995) *Biospectroscopy 1*, 207−216.
5. Goossens, K., Smeller, L., Frank, J., and Heremans, K. (1996) *Eur. J. Biochem. 236*, 254−262.
6. Panick, G., Malessa, R., Winter, R., Rapp, G., Frye, K. J., and Royer, C. A. (1998) *J. Mol. Biol. 275*, 389−402.
7. Takeda, N., Nakano, K., Kato, M., and Taniguchi, Y. (1998) *Biospectroscopy 4*, 209−216.
8. Samarasinghe, S. D., Cambell, D. M., Jonas, A., and Jonas, J. (1992) *Biochemistry 31*, 7773−7778.
9. Royer, C. A., Hinck, A. P., Loh, S. N., Prehoda, K. E., Peng, X., Jonas, J., and Markley, J. L. (1993) *Biochemistry 32*, 5222−5232.
10. Zhang, J., Peng, X., Jonas, A., and Jonas, J. (1995) *Biochemistry 34*, 8631−8641.
11. Yamaguchi, T., Yamada, H., and Akasaka, K. (1995) *J. Mol. Biol. 250*, 689−694.
12. Nash, D., Lee, B.-S., and Jonas, J. (1996) *Biochim. Biophys. Acta 1297*, 40−48.
13. Akasaka, K., Tezuka, T., and Yamada, H. (1997) *J. Mol. Biol. 271*, 671−678.
14. Li, H., Yamada, H., and Akasaka, K. (1998) *Biochemistry 37*, 1167−1173.
15. Kitchen, D. B., Reed, L. H., and Levy, R. M. (1992) *Biochemistry 31*, 10083−10093.
16. Brunne, R. M., and van Gunsteren, W. F. (1993) *FEBS Lett. 323*, 215−217.
17. Wroblowski, B., Diaz, J. F., Heremans, K., and Engelborghs, Y. (1996) *Proteins: Struct., Funct., Genet. 25*, 446−455.
18. Dong, A., Huang, P., and Caughey, W. S. (1990) *Biochemistry 29*, 3303−3308.
19. Wong, P. T. T., and Heremans, K. (1988) *Biochim. Biophys. Acta 956*, 1−9.
20. Linderstrøm-Lang, K. U. (1955) *Chem. Soc. Spec. Publ. 2*, 1−20.
21. Hvidt, A., and Nielsen, N. W. (1966) *Adv. Protein Chem. 21*, 287−386.
22. Woodward, C. K., Simon, I., and Tuchsen, E. (1982) *Mol. Cell. Biochem. 48*, 135−160.
23. Englander, S. W., and Kallenbach, N. R. (1983) *Q. Rev. Biophys. 16*, 521−655.
24. Wagner, G., and Wüthrich, K. (1986) *Methods Enzymol. 131*, 307−326.
25. Kanaya, S., Katsuda, C., Kimura, S., Nakai, T., Kitakuni, E., Nakamura, H., Katayanagi, K., Morikawa, K., and Ikehara, M. (1991) *J. Biol. Chem. 266*, 6038−6044.
26. Kanaya, S., Oobatake, M., Nakamura, H., and Ikehara, M. (1993) *J. Biotechnol. 28*, 117−136.
27. Kimura, S., Oda, Y., Nakai, T., Katayanagi, K., Kitakuni, E., Nakai, C., Nakamura, H., Ikehara, M., and Kanaya, S. (1992) *Eur. J. Biochem. 206*, 337−343.
28. Kimura, S., Nakamura, H., Hashimoto, T., Oobatake, M., and Kanaya, S. (1992) *J. Biol. Chem. 267*, 21535−21542.
29. Kimura, S., Kanaya, S., and Nakamura, H. (1992) *J. Biol. Chem. 267*, 22014−22017.
30. Ishikawa, K., Kimura, S., Kanaya, S., Morikawa, K., and Nakamura, H. (1993) *Protein Eng. 6*, 85−91.
31. Ishikawa, K., Nakamura, H., Morikawa, K., and Kanaya, S. (1993) *Biochemistry 32*, 6171−6178.
32. Ishikawa, K., Nakamura, H., Morikawa, K., Kimura, S., and Kanaya, S. (1993) *Biochemistry 32*, 7136−7142.
33. Haruki, M., Noguchi, E., Akasako, A., Oobatake, M., Itaya, M., and Kanaya, S. (1994) *J. Biol. Chem. 269*, 26904−26911.
34. Haruki, M., Noguchi, E., Nakai, C., Liu, Y.-Y., Oobatake, M., Itaya, M., and Kanaya, S. (1994) *Eur. J. Biochem. 220*, 623−631.

35. Akasako, A., Haruki, M., Oobatake, M., and Kanaya, S. (1995) *Biochemistry 34*, 8115−8122.
36. Kanaya, S., Oobatake, M., and Liu, Y. (1996) *J. Biol. Chem. 271*, 32729−32736.
37. Akasako, A., Haruki, M., Oobatake, M., and Kanaya, S. (1997) *J. Biol. Chem. 272*, 18686−18693.
38. Oobatake, M., Hashimoto, T., Nakamura, H., and Kanaya, S. (1993) *Protein Eng. 6*, 1023.
39. Kanaya, E., and Kanaya, S. (1995) *J. Biol. Chem. 270*, 19853−19860.
40. Yamasaki, K., Ogasawara, K., Yutani, K., Oobatake, M., and Kanaya, S. (1995) *Biochemistry 34*, 16552−16562.
41. Katayanagi, K., Miyagawa, K., Matsushima, M., Ishikawa, M., Kanaya, S., Ikehara, M., Matsuzaki, T., and Morikawa, K. (1990) *Nature 347*, 306−309.
42. Katayanagi, K., Miyagawa, M., Matsushima, M., Ishikawa, M., Kanaya, S., Nakamura, H., Ikehara, M., Matsuzaki, T., and Morikawa, K. (1992) *J. Mol. Biol. 223*, 1029−1052.
43. Yang, W., Hendrickson, W. A., Crouch, R. J., and Satow, Y. (1990) *Science 249*, 1398−1405.
44. Yamazaki, T., Yoshida, M., Kanaya, S., Nakamura, H., and Nagayama, K. (1991) *Biochemistry 30*, 6036−6047.
45. Yamazaki, T., Yoshida, M., and Nagayama, K. (1993) *Biochemistry 32*, 5656−5669.
46. Oda, Y., Yoshida, M., and Kanaya, S. (1993) *J. Biol. Chem. 268*, 88−92.
47. Oda, Y., Yamazaki, T., Nagayama, K., Kanaya, S., Kuroda, Y., and Nakamura, H. (1994) *Biochemistry 33*, 5275−5284.
48. Yamasaki, T., Kanaya, S., and Oobatake, M. (1995) *Thermochim. Acta 267*, 379−388.
49. Yamasaki, K., Akasako-Furukawa, A., and Kanaya, S. (1998) *J. Mol. Biol. 277*, 707−722.
50. Chamberlain, A. K., Handel, T. M., and Marqusee, S. (1996) *Nat. Struct. Biol. 3*, 782−787.
51. Dabora, J. M., Pelton, J. G., and Marqusee, S. (1996) *Biochemistry 35*, 11951−11958.
52. Raschke, T. M., and Marqusee, S. (1997) *Nat. Struct. Biol. 4*, 298−304.
53. Yamasaki, K., Saito, M., Oobatake, M., and Kanaya, S. (1995) *Biochemistry 34*, 6587−6601.
54. Wong, P. T. T., Moffatt, D. J., and Baudais, F. L. (1985) *Appl. Spectrosc. 39*, 733−735.
55. Baum, J., Dobson, C. M., Evans, P. A., and Hanley, C. (1989) *Biochemistry 28*, 7−13.
56. Bodenhausen, G., and Ruben, D. J. (1980) *Chem. Phys. Lett. 69*, 185−199.
57. Shaka, A. J., Barker, P. D., and Freeman, R. (1985) *J. Magn. Reson. 64*, 547−552.
58. Marion, D., and Wüthrich, K. (1983) *Biochem. Biophys. Res. Commun. 113*, 967−974.
59. Levenberg, K. (1944) *Q. Appl. Math. 2*, 164−168.
60. Marquardt, D. (1963) *SIAM J. Appl. Math. 11*, 431−441.
61. Kamath, U., and Shriber, J. W. (1989) *J. Biol. Chem. 264*, 5586−5592.
62. Palmer, A. G., III, Rance, M., and Wright, P. E. (1991) *J. Am. Chem. Soc. 113*, 4371−4380.
63. Bai, Y., Milne, J. S., Mayne, L., and Englander, S. W. (1993) *Proteins: Struct., Funct., Genet. 17*, 75−86.
64. Carter, J. V., Knox, D. G., and Rosenberg, A. (1978) *J Biol. Chem. 25*, 1947−1953.
65. Millero, F. J., Hoff, E. V., and Kahn, L. (1972) *J. Solution Chem. 1*, 309−327.
66. Kanaya, S., Kimura, S., Katsuda, C., and Ikehara, M. (1990) *Biochem. J. 271*, 59−66.
67. Byler, D. M., and Susi, H. (1986) *Biopolymers 25*, 469−487.
68. Susi, H., and Byler, D. M. (1988) *Appl. Spectrosc. 42*, 819−826.
69. Kennedy, D. F., Crisma, M., Toniolo, C., and Chapman, D. (1991) *Biochemistry 30*, 6541−6548.
70. Torii, H., and Tasumi, M. (1992) *J. Chem. Phys. 96*, 3379−3387.
71. Arrondo, J. L. R., Blanco, F. J., Serrano, L., and Goni, F. M. (1996) *FEBS Lett. 384*, 35−37.
72. Chirgadze, Y. N., Fedorov, O. V., and Trushina, N. P. (1975) *Biopolymers 14*, 679−694.
73. Matsuura, H., Hasegawa, K., and Miyazawa, T. (1986) *Spectrochim. Acta 42A*, 1181−1192.
74. Halloway, P. W., and Mantsch, H. H. (1989) *Biochemistry 28*, 931−935.
75. Prestrelski, S. J., Byler, D. M., and Thompson, M. P. (1991) *Int. J. Pept. Protein Res. 37*, 508−512.
76. Prestrelski, S. J., Byler, D. M., and Liebman, M. N. (1992) *Proteins: Struct., Funct., Genet. 14*, 440−450.
77. Jackson, M., Haris, P. I., and Chapman, D. (1989) *Biochim. Biophys. Acta 998*, 75−79.
78. Kuwajima, K. (1989) *Proteins: Struct., Funct., Genet. 6*, 87−103.
79. Ptitsyn, O. B. (1992) in *Protein Folding* (Creighton, T. E., Ed.) pp 243−300, W. H. Freeman and Co., New York.
80. Kanaya, S., Kohara, A., Miyagawa, M., Matsuzaki, T., Morikawa, K., and Ikehara, M. (1989) *J. Biol. Chem. 264*, 11546−11549.
81. Dill, K., Bromberg, S., Yue, K., Fiebig, K. M., Yee, D. P., Thomas, P. D., and Chan, H. S. (1995) *Protein Sci. 4*, 561−602.
82. Ptitsyn, O. B. (1987) *J. Protein Chem. 6*, 273−293.
83. Shakhnovich, E. I., and Finkelstein, A. V. (1989) *Biopolymers 28*, 1667−1680.
84. Evans, P. A., Topping, K. D., Woolfson, D. N., and Dobson, C. M. (1991) *Proteins: Struct., Funct., Genet. 9*, 248−266.
85. Saab-Rincón, G., Froebe, C. L., and Matthews, C. R. (1993) *Biochemistry 32*, 13981−13990.
86. Alexandrescu, A. T., Ecans, P. A., Pitkeathly, M., Baum, J., and Dobson, C. M. (1993) *Biochemistry 32*, 1707−1718.
87. Schulman, B. A., and Kim, P. S. (1996) *Nat. Struct. Biol. 3*, 682−687.
88. Neri, D., Billeter, M., Wider, G., and Wüthrich, K. (1992) *Science 257*, 1559−1563.
89. Lumb, K. J., and Kim, P. S. (1994) *J. Mol. Biol. 236*, 412−420.
90. Jeng, M.-F., Englander, S. W., Elöve, G. A., Wand, A. J., and Roder, H. R. (1990) *Biochemistry 29*, 10433−10437.
91. Chyan, C.-L., Wormald, C., Dobson, C. M., Evans, P. A., and Baum, J. (1993) *Biochemistry 32*, 5681−5691.
92. Buck, M., Radford, S. E., and Dobson, C. M. (1994) *J. Mol. Biol. 237*, 247−254.
93. Schulman, B. A., Redfield, C., Peng, Z., Dobson, C. M., and Kim, P. S. (1995) *J. Mol. Biol. 253*, 651−657.
94. Hughson, F. M., Wright, P. E., and Baldwin, R. L. (1990) *Science 249*, 1544−1548.
95. Kraulis, P. J. (1991) *J. Appl. Crystallogr. 24*, 946−950.
96. Ooi, T., and Oobatake, M. (1988) *J. Biochem. (Tokyo) 104*, 440−444.
97. Oobatake, M., and Ooi, T. (1993) *Prog. Biophys. Mol. Biol. 59*, 237−284.

BI981046W